Molecular speciation and dynamics of oxidized triacylglycerols in lipid droplets: Mass spectrometry and coarse-grained simulations

Dariush Mohammadyani[a,b,c], **Vladimir A. Tyurin**[a,c], **Matthew O'Brien**[d], **Yoel Sadovsky**[d], **Dmitry I. Gabrilovich**[e], **Judith Klein-Seetharaman**[f], and **Valerian E. Kagan**[a,c,*]

[a]Department of Environmental and Occupational Health, University of Pittsburgh, Pittsburgh, PA 15219, USA

[b]Department of Bioengineering, University of Pittsburgh, Pittsburgh, PA 15219, USA

[c]Center for Free Radical and Antioxidant Health, University of Pittsburgh, Pittsburgh, PA 15219, USA

[d]Magee–Womens Research Institute, University of Pittsburgh, Pittsburgh, PA 15219, USA

[e]The Wistar Institute, Philadelphia, PA 19104, USA

[f]Division of Metabolic and Vascular Health, Medical School, University of Warwick, Coventry CV4 7AL, UK

Abstract

Lipid droplets (LDs) are ubiquitous and physiologically active organelles regulating storage and mobilization of lipids in response to metabolic demands. Among the constituent LD neutral lipids, such as triacylglycerols, cholesterol esters, and free fatty acids, oxidizable polyunsaturated molecular species may be quite abundant, yet the structural and functional roles of their oxidation products have not been studied. Our previous work documented the presence of these peroxidized species in LDs. Assuming that hydrophilic oxygen-containing functionalities may markedly change the hydrophobic/hydrophilic molecular balance, here we utilized computational modeling to test the hypothesis that lipid peroxidation causes redistribution of lipids between the highly hydrophobic core and the polar surface (phospho) lipid monolayer–the area enriched with integrated enzymatic machinery. Using quantitative liquid chromatography/mass spectrometry, we characterized molecular speciation of oxTAGs in LDs of dendritic cells in cancer and hypoxic trophoblasts cells as two cellular models associated with dyslipidemia. Among the many types of oxidized lipids identified, we found that oxidatively truncated forms and hydroxyl derivatives of TAGs were the prevailing oxidized lipid species in LDs in both cell types. Using coarse grained molecular dynamics (CG-MD) simulations we established that lipid oxidation changed their partitioning whereby oxidized lipids migrated into the outer monolayer of the LD, where they can

---

*Corresponding author at: University of Pittsburgh, Departments of Environmental and Occupational Health, Pittsburgh, PA 15219, USA. Fax: +1 412 624 9361. kagan@pitt.edu (V.E. Kagan).

affect essential metabolic pathways and undergo conversions, possibly leading to the formation of oxygenated lipid mediators.

Keywords

Lipid droplet; Neutral lipids; Lipid oxidation; Hypoxia; Cancer

Introduction

Lipid droplets (LDs) are dynamic cytoplasmic organelles that can be found in nearly all eukaryotic cells [1,2]. They play important roles during changes in metabolism of intracellular neutral lipids, particularly free fatty acids [3]. Not surprisingly, LDs have been related to dyslipidemias that are characteristic of a number of chronic diseases, including obesity, diabetes, atherosclerosis, and the metabolic syndrome [4–7]. The structural organization and function of LDs are determined by the physico-chemical intermolecular interactions of neutral lipids with each other in the hydrophobic core and with phospholipids, particularly phosphatidylcholine (PC), as well as with proteins embedded in the surface monolayer [1]. The number of PCs and other polar molecules available to cover sufficient surface area of the LD defines its overall size in the aqueous cytosolic environment [8,9]. Moreover, the surface monolayer, along with its enzymatic machinery and corresponding adapter proteins, is viewed as a locale of metabolic conversions of constituting LD lipids [10,11].

Among the neutral lipids comprising the hydrophobic core, triacylglycerols (TAGs), cholesterol esters (ChEs), and free fatty acids (FFAs)–in different proportions–are the most prominent components of LDs [12]. While the composition and molecular identities of neutral lipids are influenced by extra- and intracellular metabolic demands, a significant proportion of these molecules may be represented by polyunsaturated species with two or more double bonds [13]. This suggests that the vulnerability to oxygenation may lead to the appearance of polar functionalities in the hydrophobic acyls, shifting the molecular hydrophobic/hydrophilic balance [14], and causing significant modifications of LDs organization. Indeed, we have recently documented the presence of oxygenated TAGs, ChEs, and FFAs in immunologically impaired dendritic cells from tumor-bearing animals and cancer patients [15–17]. Reasoning that these oxidative modifications of polyunsaturated fatty acid (PUFA)-containing LDs may be widespread, here we undertook a combined mass spectrometry (MS) and computational molecular dynamics (MD) study of the effects triggered by the appearance of oxidized TAGs (oxTAGs) in LDs. Given the myriads of possible diversified oxygenated TAGs, our choice was based on the LC-MS-based detection of these species in two types of cells–dendritic cells of tumor-bearing mice and primary human placental trophoblasts–which accumulate LDs as a consequence of hypoxia-induced dyslipidemia [18]. Considering the relatively large total number of atoms in a typical LD that comprises several hundred lipid molecules, coarse-grained molecular dynamics (CG-MD) simulations, rather than full atomistic MD simulations, offer advantages of greater length and time scales for characterizing the dynamic behavior of oxidized lipids [19]. We demonstrate that oxTAGs affect the hydrophobic–hydrophilic balance of LDs,

leading to disturbances in phase separation between the neutral lipid core and the phospholipid outer monolayer.

Methods

Mass spectroscopy analysis of LD composition

We used two tumor cell lines, EL4 lymphoma and MC 38 colon carcinomas, maintained in Dulbecco's modified eagle's medium (Invitrogen Corp. Carlsbad, CA) plus 10% fetal bovine serum (FBS, Sigma-Aldrich) at 37 °C, 5% CO_2. DCs were generated from bone marrow progenitor cells using culture with 10 ng/mL recombinant mouse GM-CSF (Invitrogen Corp), and 10 ng/mL interleukin 4 (R&D Systems) as described previously [15]. Tumor explants were prepared from freshly isolated subcutaneous tumors [15]. *In vivo*, dendritic cells (DCs) were purified from spleen of C57BL/6 naïve tumor-free and EL-4 tumor bearing mice using biotinylated CD11c specific antibody (BD Pharmingen) and magnetic beads (Miltenyi Biotec). For *in vitro* generation of DCs, hematopoietic progenitor cells were isolated from bone marrow of tumor-free mice using a lineage cell depletion kit (Miltenyi Biotec) and cultured for 3 days in completed RPMI1640 medium supplemented 10% FBS, antibiotics, and 10 ng/mL granulocyte macrophage colony stimulated factor (Peprotech). Then, the medium was replaced with the one containing 20% v/v tumor explant spleen (TES). After 2 additional days of incubation, DCs were isolated using CD11c antibody and magnetic beads.

Isolation of trophoblast cells and lipid droplets

Primary human trophoblasts (PHT cells) were isolated from healthy singleton term placentas using the trypsin-DNase-dispase/Percoll method as described by Kliman et al., with previously published modifications [20] under an exempt protocol approved by the Institutional Review Board at the University of Pittsburgh. PHT cells were cultured up to 72 h under standard conditions of 20% oxygen. For induction of LD, trophoblasts were cultured between 24 and 72 in hermetically enclosed incubators that supply $O_2 < 1\%$, as we previously described [21]. Formation of trophoblast lipid droplets was examined and confirmed using BODIPY 493/503 (Invitrogen/Molecular Probes, Eugene, OR). Isolation of lipid droplets fractions was performed as previously described [22].

Analysis of lipids

Total lipids were extracted from cells by the Folch procedure [23] and analyzed by a Dionex Ultimate 3000 HPLC coupled online to a linear ion trap mass spectrometer (LXQ Thermo-Fisher). Simultaneous LC/ESI-MS analysis of free fatty acids and their oxidation products was performed as we previously published [17]. The LC/ESI-MS analysis of TAG was performed using gradient solvents as previously described [15,16], including A, methanol, and B, 2-propanol containing 0.1% ammonium hydroxide. The column was eluted during the first 6 min using a linear gradient 0–3% solvent B, from 6 to 18 min isocratic at 3% solvent B, from 18 to 35 min with a linear gradient from 3 to 40% solvent B, then 35–40 min isocratic using 40% solvent B, 40–80 min with a linear gradient from 40 to 55% solvent B, 80–83 min isocratic using 55% solvent B, then 83–85 min with linear gradient 55–0% solvent B, 85–90 min isocratic at 0% solvent B for equilibration of the column. MS spectra

were acquired in positive ion mode, using range zoom (500– 1000 m/z). TAG cations were formed through molecular ammonium adduction (TAG + NH$_4$). Positional analysis of acyl chains in TAG species was performed after CID fragmentation of TAGs [24,25]. The spectra of cholesterol esters (CE) were also acquired in positive ion mode on a hybrid quadrupole-orbitrap mass spectrometer (Q-Exactive, ThermoFisher, Inc., San Jose, CA). Phospholipids were analyzed as previously described [26].

To quantitatively assess lipid contents, the following standards were used: oxFFA (9-hydroperoxy-10E,12Z-octadecadienoic acid, 13-hydroperoxy-9Z,11E- octadecadienoic acid, 9-hydroxy-10E,12Z-octadecadienoic acid, 13-hydroxy-9Z, 11E-octadecadienoic acid, 9-oxo-10E,12Z-octadecadienoic acid, 13-oxo-9Z,11E- octadecadienoic acid, 9(10)-epoxy-12Z-octadecenoic acid, 9,10-EpOME, 12(13) epoxy-9Z- octadecenoic acid), oxidized cholesterol esters, ((±)-9-hydroxy-10E,12Z-octadecadienoic acid, cholesteryl ester, (±)-9-hydroperoxy-10E,12 Z-octadecadienoic acid, cholesteryl ester; (±)-13-hydroperoxy-9Z,11 E-octadecadienoic acid, cholesteryl ester), and oxTAGs (linolein hydroperoxides, hydroxy linoleins) from Cayman Chemicals (Ann Arbor, MI); TAG internal and reference standards from Supelco (Bellefonte, PA), and phospholipids from Avanti Polar Lipids Inc. (Alabaster, AL).

Statistical analysis was performed by either paired/unpaired Student's t test or one-way ANOVA. Significance was set at $P < 0.05$. The results are presented as mean values ± SD, derived from at least three experiments.

Setup and optimization of CG model of LD

Coarse-grained simulations were based on the Martini force field [17]. In this approach, four heavy atoms are mapped to one CG bead. Two hundred triacylglycerol molecules with linoleic fatty acids acyl chains were used to construct the LD core, and 1-palmitoyl-2-oleoyl-sn-glycero-3-phosphocholine (POPC) to construct the outer monolayer. The CG models of TAG and POPC molecules are illustrated in Fig. S1A. To create the optimized LD model, we investigated the effect of varying the relative ratio between TAGs and phospholipids on the shape of the resulting LD model. Four different POPC:TAG ratios of 1, 2, 3, and 4 were chosen and subjected to simulation (Fig. S1B). The resulting shapes of the LDs with different lipid compositions, as inspected after 50 ns equilibration, are summarized in Fig. S1C.

CG-MD simulations of LD containing oxTAGs

The effects of adding oxidatively truncated- and dihydroxy-TAGs to the LD core on lipid partitioning in LDs were evaluated using CG-MD simulations with the optimized LD model containing 200 TAG and 400 POPC molecules (Fig. S1B, Panel III). Two different levels of oxidation have been assessed, 5 and 10 mol% oxTAGs. As controls, we simulated LDs without adding any oxidized TAG species. Thus, five fully hydrated systems were set up (Table S1). For each of the five systems, three different simulations were carried out by equilibrating them with three different random seeds to produce different initial velocities and thus different trajectories. In total, 15 simulations were run, 2 μs each. All simulations were performed using the GROMACS v. 4.5.4 MD package [27] and visualized using VMD

v. 1.9 software [28]. Initially, each system was minimized for 20 ps, before 2 ns NVT ensemble equilibration. A 40 fs time step was used to integrate the equations of motion. Nonbonded interactions have a cutoff distance of 1.2 nm. Temperature and pressure were controlled using the velocity rescale (V rescale) [29] and Berendsen [30] algorithms, respectively. Simulations were run at 300 K and at 1 atm during NPT runs.

Results

Quantification of TAGs in model cell systems

Disturbances in synthesis, uptake, and oxidative catabolism of free fatty acids, including polyunsaturated fatty acids, can lead to their elevated steady-state intracellular concentrations. This may trigger esterification reactions, yielding predominantly TAGs and ChEs, and resulting in the formation of LDs [31]. The PUFA-containing esterified products may be a source of peroxidized species, affecting LD structure. We chose two different nonadipose cell models that characteristically accumulate LDs: (i) DCs from tumor-bearing animals with elevated levels of CD204 receptor, known to avidly uptake and accumulate lipids from plasma [15,16], and (ii) hypoxic trophoblasts, in which impaired FA oxidation and trafficking are mostly responsible for the dyslipidemia [18]. In both cases, TAGs were quantitatively the most abundant species of accumulated neutral lipids, accountable for at least 65–70% of their total content [15,16,18]. We performed LC-MS analysis of TAGs in these two cell types compared to their respective controls, and established a significantly elevated content of TAGs (including PUFA-containing species of TAGs) (Fig. 1, Table 1).

Molecular characterization of oxidized TAGs

Next, we established the molecular identity and determined the respective abundance of peroxidation products of TAGs. In DCs from tumor-bearing mice, the major types of oxTAGs were represented by a variety of oxygenated species including monohydroxy and dihydroxy species [16,17]. Interestingly, normal DCs isolated from bone marrow of naïve mice contained barely detectable levels of oxidized LA (oxLA). However, EL-4 TES or MC38 TES (data not shown) accumulated large amounts of oxLA, represented by oxo, monohydroxy, and dihydroxy derivatives (data not shown) and a variety of monooxygenated and oxidatively truncated species of oxTAGs (Fig. 2). Monooxygenated oxTAGs with *m/z* at 912, 914, 916, and 918 corresponded to molecular species 54:6; 54:5; 54:4; 54:3 containing C18:2/C18+O/C18:2; C18:1/C18:2+O/C18:2; C18:1/C18:2+O/C18:1; and C18:1/C18:2+O/C18:0 fatty acid residues, respectively (Fig. 2A). Oxidatively truncated TAGs–with *m/z* 710, 712, 738, 740, 764, and 766– contained 7-oxo-heptanoic or 9-oxo-nonanoic acid residues generated by oxidative cleavage of LA, and corresponded to molecular species 39:1; 39:0; 41:1; 41:0; 43:2; 43:1, respectively (Fig. 2B). The total abundance of these species was as high as 340 pmol/10^6 cells, which corresponded to $\sim$ 14 mol% of total TAGs.

We also detected oxidatively modified polyunsaturated TAGs, represented by mono-, dioxygenated, and oxidatively truncated molecular species, in LDs isolated from hypoxic PHT cells (Fig. 3, Fig. S2). Fragmentation analysis of mono- and dioxygenated oxTAGs at *m/z* 890 and 906 confirmed that they corresponded to 52:3 molecular species with C16:0/C18:2 + O/C18:1 and C16:0/C18:2+2O/C18:1 fatty acids, which originated from TAG

molecular species 52:3 at *m/z* 784 containing C16:0/C18:2/C18:1 fatty acids. The major molecular species of oxidatively truncated oxTAG were observed at *m/z* 712, 740, and 766 and corresponded to 39:0; 41:0, and 43:1 species that included 9-oxo-nonanoic acid C12:0/ C9oxo:0/C18:0, C14:0/C9oxo:0/C16:0; C14:0/C19oxo:0/C18:0, C16:0/C9oxo:0/C16:0; and C16:0/C9oxo:0/C18:1, C16:1/C9oxo:0/C18:0, respectively (Fig. 3). Notably, oxTAGs were not detected in PHT cells cultured under normoxic conditions.

Development of a CG-MD model for LDs

CG-MD modeling has been successfully applied to studies of lipoproteins–HDL and LDL [32–34]–but not generic LDs. We therefore first developed and optimized a model for a LD without oxTAGs. In the initial simulations, we assessed the effects of varying the POPCTAG ratios at a fixed number of TAGs on LD organization after 50 ns equilibration (Fig. S1). The LDs shape was strongly dependent on the number of POPC molecules present. When the number of POPC was too high, elongated shapes were observed, and when the number of POPC was too low, there was not sufficient POPC to cover the surface of the LD. Only at a POPCTAG ratio of 2, the characteristic spherical shape and two distinctively separated phases of core and surface monolayer were achieved. This equilibrated arrangement of LDs remained stable within 2 μs (Fig. 4A) at which point several TAG molecules were found to be partitioned from the hydrophobic core into the more polar regions of the PC monolayer. Analysis of 1D and 2D number density graphs (Fig. 4B and C, respectively) along the *z*-direction established that the approximate boundary of the LD core and monolayer was located at *r*= ~4 nm.

Effects of lipid oxidation on lipids dynamics in LD

To study the effect of lipid oxidation on lipid dynamics in LD, we used the LC-MS data to guide us in the choice of molecular species and the amounts of oxidized lipids to be modeled. LDs containing two representative types of oxidized TAGs–with hydroxy-LA and oxidatively truncated LA–at two different oxidization levels (5 and 10 mol% of total TAGs) have been employed in the CG-MD simulations (Fig. 5). When compared to nonoxidized TAGs, we found that a significantly larger amount of oxidatively modified TAGs of both types partitioned into the phospholipid monolayer. 1D number density graphs of oxidatively truncated TAG displayed two shoulders on both sides of the graph, clearly revealing their tendency to partition into the PC monolayer (Fig. 6A). 2D number density maps of oxTAGs uniformly confirmed their preferred redistribution from the hydropbobic core into the more polar surface monolayer (Fig. 6B). Similar behavior was observed for LDs containing dihydroxy-TAG species (Fig. S3). To compare the dynamics of nonoxidized TAGs and oxTAGs, 2D number density maps of TAGs for the entire system were generated (Fig. S4). They demonstrated that nonoxidized TAGs preferentially located in the core region. The expanded view of the final configurations showed that TAGs and oxTAGs in the monolayer were located below the head groups of POPC molecules (Fig. S5A) and they distributed arbitrarily, without detectable clustering (Fig. S5B). The dynamics of several randomly selected oxTAGs and TAGs revealed that unlike TAGs, the oxTAGs preferred to remain in the monolayer (Fig. S6).

Discussion

LDs are essential for the regulation of lipid homeostasis in both adipose and nonadipose tissues [4]. The dynamic features of LDs as organelles capable of changing their neutral lipids content in adaptive response to metabolic demands and conditions are maintained by a large number of catabolic and anabolic enzymes. These enzymatic assemblies are localized on the LD surfaces, and play a role in the regulatory interface between the hydrophobic core and the aqueous cytosol, as well as in membranes of other organelles, particularly endoplasmic reticulum and mitochondria [35]. Amphiphilic phospholipids, adsorbed at the interface between the interior of the LD and the surface as a monolayer, are essential for decreasing LD surface tension, creating high bending elasticity, stability, and most importantly allowing the accommodation and organization of the enzymatic lipid-metabolizing machinery [36]. The thorough control over the amounts of interface molecules between the two phases is critical to the cellular function of LDs. Notably, oxidizable PUFA-TAGs may constitute a significant fraction of the total amounts of neutral lipids in LDs. Our LC-MS data indicate that in both types of cells–DCs and trophoblasts–the oxidizable species were accountable for > 60% of their total content. Remarkably, in both cases we detected significant amounts of oxidized TAGs that harbored oxygenated functionalities such as monooxygenated and dioxygenated derivatives as well as oxidatively truncated TAG species. Although their origin and mechanisms of their formation remain to be elucidated, the appearance of TAGs with these polar oxygenated groups in the hydrophobic core on LDs may act as an important factor shifting the equilibrium properties of the LD where the perturbed balance between hydrophobic and hydrophilic groups results in altered distributions of the constituent lipids.

Although lipid peroxidation has not been studied in LDs, their effects on membranes have been investigated previously [37,38]. In particular, it has been shown that the addition of polar oxygen atom (s) to fatty acyl chains of phospholipids causes reorientation of the modified acyl chain, and results in its protrusion into the aqueous phase like "whiskers" [37,38]. This finding suggests that peroxidation increases the affinity of hydrophobic lipid acyls for the polar aqueous phase. Indeed, our computational modeling of LDs containing oxidized neutral lipids indicated that the presence of oxTAGs inside the hydrophobic LD was thermodynamically unstable, resulting in their migration toward the hydrophilic surface. Both oxidatively truncated TAGs and dihydroxy-TAGs disturbed the stability of the two distinctive LD phases, and their presence causes partitioning of oxTAGs into the phospholipid monolayer. Notably, increasing the content of oxTAGs from 5 to 10 mol% enhanced the partitioning of oxTAGs into the POPC monolayer.

As a lipid storage organelle [39], the neutral lipids deposited in the LD hydrophobic core should have access to lipases that facilitates their metabolism. Walther and Farese [39] hypothesized that this can be achieved via: (i) an "extension" of lipases through the phospholipid monolayer to reach the required bonds of neutral lipids, or (ii) penetration of neutral lipids in the PC monolayer. Our computer modeling data are compatible with the second hypothesis. Indeed, we found that a small fraction of nonoxidized TAGs also moved to the POPC monolayer. This is in line with a previous study [32] showing that in HDL also

cholesterol esters were able to penetrate into the outer monolayer to reach to the ChE transferase protein, apolipoprotein A-1, on the surface.

The closed-up snapshots of LD after 2 μs (Fig. S5A) demonstrated the presence of both oxTAGs and TAGs in close proximity to the LD surface, immediately below the choline and phosphate groups of POPC molecules. This suggests that the "sensitive" bonds of these TAGs may be accessible to LD-associated proteins. Notably, although both TAGs and oxTAGs are capable of moving into the POPC monolayer, the latter preferentially stay for a longer time in the proximity of the phospholipid monolayer over the entire time of the trajectory, while the former are not stable in the outer monolayer and fluctuate between the two LD phases.

Are the dynamics of oxTAGs and their partitioning into the LD monolayer physiologically relevant? The accumulation and presence of oxidized neutral lipids in the LD monolayer suggest their potential roles in lipid mediator signaling networks. Indeed, lipolysis of oxTAGs should generate oxFFAs–precursors of lipid mediators. Despite the fact that this study presents a simplified model of oxidized lipid dynamics in LD, our data suggest novel mechanisms of biochemical processing of TAGs and oxTAGs that raise challenging biophysical questions. For instance, it has been suggested that trophoblast dysfunction in hypoxia is associated with enhanced lipid peroxidation [40]. Moreover, oxidized FFAs activate proteins that impact trophoblast homeostasis [41]. However, the molecular pathways through which these important pathological processes occur remain to be elucidated. Similarly, the role of oxTAG migration to the surface of the phospholipid-covered monolayer in aberrant cross-presentation of antigens by dendritic cells of tumor-bearing animals is still enigmatic.

Our CG-MD demonstration of preferred partitioning of oxidatively modified neutral lipids to the surface area is based on a model which corresponds to a relatively small LD size compared to the actual LD dimensions. Thus, our model depicts a higher curvature and a higher surface pressure at the interface, which can be addressed in future studies.

In conclusion, we found that TAGs with oxidatively modified PUFA constitute ~ 10% of the total amount of these neutral lipids in LDs in two types of cells–DCs in cancer and hypoxic human trophoblasts [41]. The appearance of polar oxygenated groups in TAGs in the hydrophobic core of LDs may be an important factor causing redistribution of LD lipids from the core toward the surface monolayer. Noteworthy, the hydrolysis of oxTAG by the LD lipases yields polyunsaturated nonoxidized and oxygenated FFA [42]. The latter can be utilized as precursors of lipid mediators with important signaling functions [43]. Therefore, the biological role and pathological significance of oxidized neutral lipid accumulation at the LD surface monolayer, a site of abundant enzymatic metabolizing lipid functions and production of oxygenated FA lipid signals, deserve further studies.

Supplementary Material

Refer to Web version on PubMed Central for supplementary material.

Acknowledgments

References

1. Fujimoto T, et al. Lipid droplets: a classic organelle with new outfits. Histochem Cell Biol. 2008; 130:263–279. [PubMed: 18546013]

2. Walther TC, Farese RV Jr. Lipid droplets and cellular lipid metabolism. Annu Rev Biochem. 2012; 81:687–714. [PubMed: 22524315]

3. Cabodevilla AG, et al. Cell survival during complete nutrient deprivation depends on lipid droplet-fueled beta-oxidation of fatty acids. J Biol Chem. 2013; 288(39):27777–27788. [PubMed: 23940052]

4. Reue K. A thematic review series: lipid droplet storage and metabolism: from yeast to man. J Lipid Res. 2011; 52(11):1865–1868. [PubMed: 21921134]

5. Puskas LG, et al. Polyunsaturated fatty acids synergize with lipid droplet binding thalidomide analogs to induce oxidative stress in cancer cells. Lipids Health Dis. 2010; 9:56. [PubMed: 20525221]

6. Stephens NA, Skipworth RJE, MacDonald AJ, Greig CA, Ross JA, Fearon KCH. Intramyocellular lipid droplets increase with progression of cachexia in cancer patients. J Cachexia Sarcopenia Muscle. 2011; 2:111–117. [PubMed: 21766057]

7. Bozzaa PT, Viola JPB. Lipid droplets in inflammation and cancer. Prostaglandins, Leukot Essent Fatty Acids. 2010; 82:243–250. [PubMed: 20206487]

8. Shi X, et al. Regulation of lipid droplet size and phospholipid composition by stearoyl-CoA desaturase. J Lipid Res. 2013; 54(9):2504–2514. [PubMed: 23787165]

9. Penno A, Hackenbroich G, Thiele C. Phospholipids and lipid droplets. Biochim Biophys Acta. 2013; 1831:589–594. [PubMed: 23246574]

10. Ducharme NA, Bickel PE. Lipid droplets in lipogenesis and lipolysis. Endocrinology. 2008; 149(3):942–949. [PubMed: 18202123]

11. Kuramoto K, et al. Perilipin 5, a lipid droplet-binding protein, protects heart from oxidative burden by sequestering fatty acid from excessive oxidation. J Biol Chem. 2012; 287(28):23852–23863. [PubMed: 22532565]

12. Murphy S, Martin S, Parton RG. Lipid droplet-organelle interactions; sharing the fats. Biochim Biophys Acta. 2009; 1791(6):441–447. [PubMed: 18708159]

13. Tobin KA, et al. Long-chain polyunsaturated fatty acid transport across human placental choriocarcinoma (BeWo) cells. Placenta. 2009; 30(1):41–47. [PubMed: 19010540]

14. Girotti AW. Lipid hydroperoxide generation, turnover, and effector action in biological systems. J Lipid Res. 1998; 39(8):1529–1542. [PubMed: 9717713]

15. Herber DL, et al. Lipid accumulation and dendritic cell dysfunction in cancer. Nat Med. 2010; 16(8):880–886. [PubMed: 20622859]

16. Cao WR, Tuyrin VA, Veglia F, Condamine T, Amoscato A, Mohammadyani D, Johnson JJ, Zhang LM, Klein-Seetharaman J, Celis E, Kagan VE, Gabrilovich DI. Oxidized lipids block antigen cross-presentation by dendritic cells in cancer. J Immunol. 2014; 192(6):2920–2931. [PubMed: 24554775]

17. Tyurin VA, et al. Mass-spectrometric characterization of peroxidized and hydrolyzed lipids in plasma and dendritic cells of tumor-bearing animals. Biochem Biophys Res Commun. 2011; 413(1):149–153. [PubMed: 21872574]

18. Biron-Shental T, et al. Hypoxia regulates the expression of fatty acid-binding proteins in primary term human trophoblasts. Am J Obstet Gynecol. 2007; 197(5):516 e1–6. [PubMed: 17826730]

19. Ingólfsson HIL, Uusitalo JJ, de Jong DH, Gopal SM, Periole X, Marrink SJ. The power of coarse graining in biomolecular simulations. WIREs Comput Mol Sci. 2013 In press.

20. Nelson DM, et al. Hypoxia limits differentiation and up-regulates expression and activity of prostaglandin H synthase 2 in cultured trophoblast from term human placenta. Am J Obstet Gynecol. 1999; 180(4):896–902. [PubMed: 10203658]

21. Oh SY, Chu T, Sadovsky Y. The timing and duration of hypoxia determine gene expression patterns in cultured human trophoblasts. Placenta. 2011; 3210(12):1004–1009. [PubMed: 21986473]

22. Brasaemle DL, Wolins NE. Isolation of lipid droplets from cells by density gradient centrifugation. Curr Protoc Cell Biol. 2006; Chap. 3:15. Unit 3. [PubMed: 18228483]

23. Folch J, Lees M, Sloane Stanley GH. A simple method for the isolation and purification of total lipides from animal tissues. J Biol Chem. 1957; 226(1):497–509. [PubMed: 13428781]

24. Li X, Evans JJ. Examining the collision-induced decomposition spectra of ammoniated triglycerides as a function of fatty acid chain length and degree of unsaturation. I. The OXO/YOY series. Rapid Commun Mass Spectrom. 2005; 19(18):2528–2538. [PubMed: 16106375]

25. Malone M, Evans JJ. Determining the relative amounts of positional isomers in complex mixtures of triglycerides using reversed-phase high-performance liquid chromatography-tandem mass spectrometry. Lipids. 2004; 39(3):273–284. [PubMed: 15233407]

26. Tyurin VA, et al. Specificity of lipoprotein-associated phospholipase A (2) toward oxidized phosphatidylserines: liquid chromatography-electrospray ionization mass spectrometry characterization of products and computer modeling of interactions. Biochemistry. 2012; 51(48): 9736–9750. [PubMed: 23148485]

27. Van Der Spoel D, et al. GROMACS: fast, flexible, and free. J Comput Chem. 2005; 26(16):1701–1718. [PubMed: 16211538]

28. Humphrey W, Dalke A, Schulten K. VMD: visual molecular dynamics. J Mol Graph. 1996; 14(1): 33–38. 27-8. [PubMed: 8744570]

29. Bussi G, Donadio D, Parrinello M. Canonical sampling through velocity rescaling. J Chem Phys. 2007; 126(1):014101. [PubMed: 17212484]

30. Berendsen HJC, et al. Molecular-dynamics with coupling to an external bath. J Chem Phys. 1984; 81(8):3684–3690.

31. Zimmermann R, et al. Fate of fat: the role of adipose triglyceride lipase in lipolysis. Biochim Biophys Acta. 2009; 1791(6):494–500. [PubMed: 19010445]

32. Vuorela T, et al. Role of lipids in spheroidal high density lipoproteins. PLoS Comput Biol. 2010; 6(10):e1000964. [PubMed: 21060857]

33. Koivuniemi A, et al. Lipid exchange mechanism of the cholesteryl ester transfer protein clarified by atomistic and coarse-grained simulations. PLoS Comput Biol. 2012; 8(1):e1002299. [PubMed: 22253581]

34. Catte A, et al. Structure of spheroidal HDL particles revealed by combined atomistic and coarse-grained simulations. Biophys J. 2008; 94(6):2306–2319. [PubMed: 18065479]

35. Kimmel AR, Sztalryd C. Perilipin 5, a lipid droplet protein adapted to mitochondrial energy utilization. Curr Opin Lipidol. 2014

36. Thiam AR, Farese RV Jr, Walther TC. The biophysics and cell biology of lipid droplets. Nat Rev Mol Cell Biol. 2013; 14(12):775–786. [PubMed: 24220094]

37. Wong-Ekkabut J, et al. Effect of lipid peroxidation on the properties of lipid bilayers: a molecular dynamics study. Biophys J. 2007; 93(12):4225–4236. [PubMed: 17766354]

38. Greenberg ME, et al. The lipid whisker model of the structure of oxidized cell membranes. J Biol Chem. 2008; 283(4):2385–2396. [PubMed: 18045864]

39. Walther TC, Farese RV Jr. The life of lipid droplets. Biochim Biophys Acta. 2009; 1791(6):459–466. [PubMed: 19041421]

40. Branch DW, et al. Pre-eclampsia and serum antibodies to oxidised low-density lipoprotein. Lancet. 1994; 343(8898):645–646. [PubMed: 7509433]

41. Schild RL, et al. The activity of PPAR gamma in primary human trophoblasts is enhanced by oxidized lipids. J Clin Endocrinol Metab. 2002; 87(3):1105–1110. [PubMed: 11889173]

42. Radner FP, et al. Growth retardation, impaired triacylglycerol catabolism, hepatic steatosis, and lethal skin barrier defect in mice lacking comparative gene identification-58 (CGI-58). J Biol Chem. 2010; 285(10):7300–7311. [PubMed: 20023287]

43. Ren R, et al. A lipid peroxidation product 9-oxononanoic acid induces phospholipase A2 activity and thromboxane A2 production in human blood. J Clin Biochem Nutr. 2013; 52(3):228–233. [PubMed: 23704812]

Abbreviations

ChEs	cholesterol esters
CG-MD	coarse-grained molecular dynamics
DCs	dendritic cells
FFAs	free fatty acids
LDs	Lipid droplets
oxTAGs	oxidized TAGs
PHT	primary human trophoblasts
PC	phosphatidylcholine
POPC	1-palmitoyl-2-oleoyl-*sn*-glycero-3-phosphocholine
TAGs	triacylglycerols
TES	tumor explant spleen
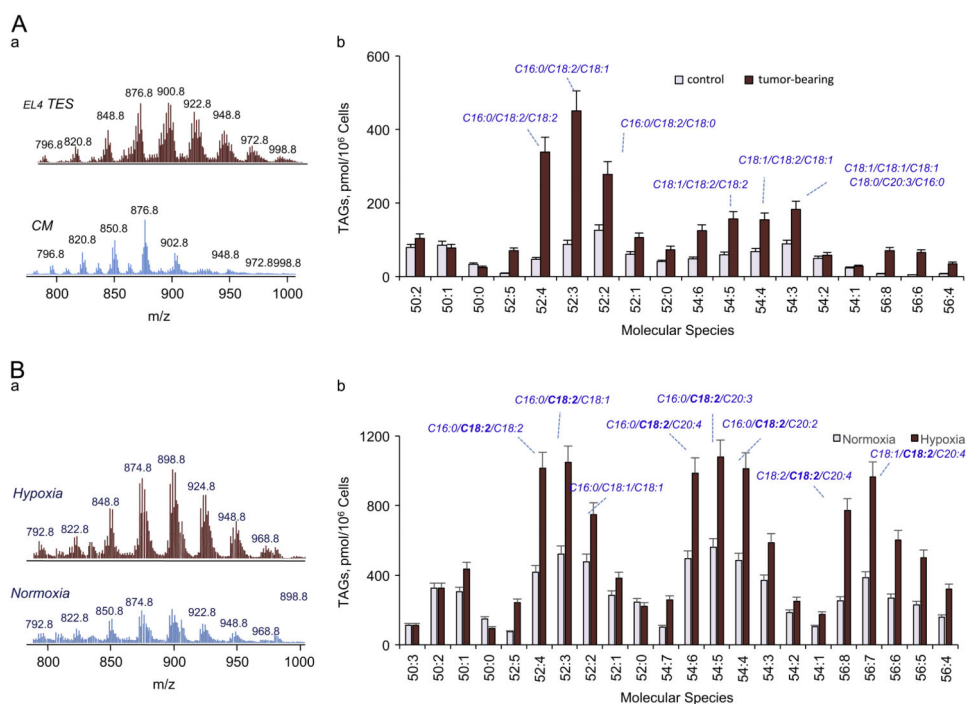
Fig. 1.
LDs contain considerable amounts of TAGs with LA acyls in DCs and PHT. A (a) MS1 spectra of TAGs from naïve DCs cultured in complete media (lower panel) and with EL4 TES (upper panel). A (b) Content of different molecular species of TAGs in control DCs from and DCs grown in EL4 TES media. B (a) MS1 spectra of TAGs from PHT cultured in normoxic conditions (lower panel) and after 24 h exposure to hypoxia (upper panel). B (b) Content of different molecular species of TAGs in control and hypoxic PHT.
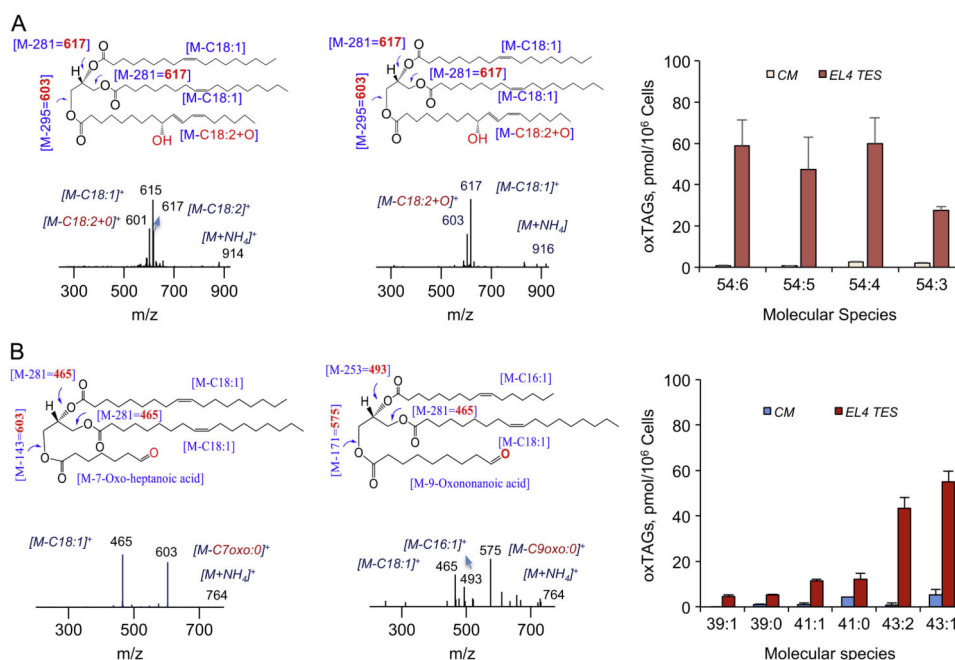
Fig. 2.

Accumulation of oxTAGs species in DCs cultured in complete medium and in EL4 TES medium. (A) Typical MS2 spectra of monooxygenated oxTAGs at *m/z* 914 and 916 (left and middle panels) corresponding to 54:5 and 54:4 molecular species containing C18:1/ C18:2+O/C18:2 and C18:1/C8:2+O/C18:1 fatty acids, respectively. Possible structures are inserted. Accumulation of monooxygenated oxTAGs species in DC cultured in EL4 TES medium (right panel). Arrows indicate fragments of oxTAGs. For example, fragmentation of the parent ion at *m/z* 914 [M+NH₄]⁺ reveals daughter ions at *m/z* 617, 615, and 601. The products ions at *m/z* 617 and 615 were formed by loss of C18:2 and C18L1 acids, respectively. The product ion at *m/z* 601 was formed by loss of oxygenated C18:2+O acid. (B) Typical MS2 spectra of truncated oxTAGs at *m/z* 764 (left and middle panels) corresponding to 43:2 molecular species containing C18:1/C7oxo:0/C18:1 and C16:1/ C9oxo:0/C18:1 fatty acids, respectively. Possible structures are inserted. Accumulation of truncated oxTAGs species in DC cultured in EL4 TES medium (right panel).
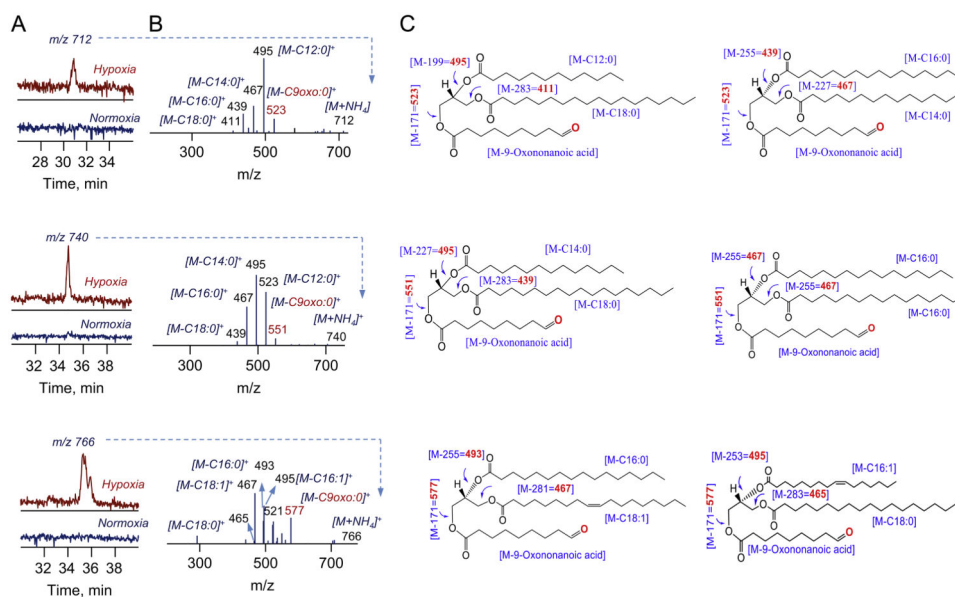
Fig. 3.
Hypoxia induced accumulation of truncated molecular species of oxTAGs in LDs from human trophoblasts. Typical LC-MS profiles (A, left panels), MS2 spectra (B, middle panels) and possible structures (*C*, right panels) of truncated oxTAGs species at *m/z* 712; 740 and 766, respectively.
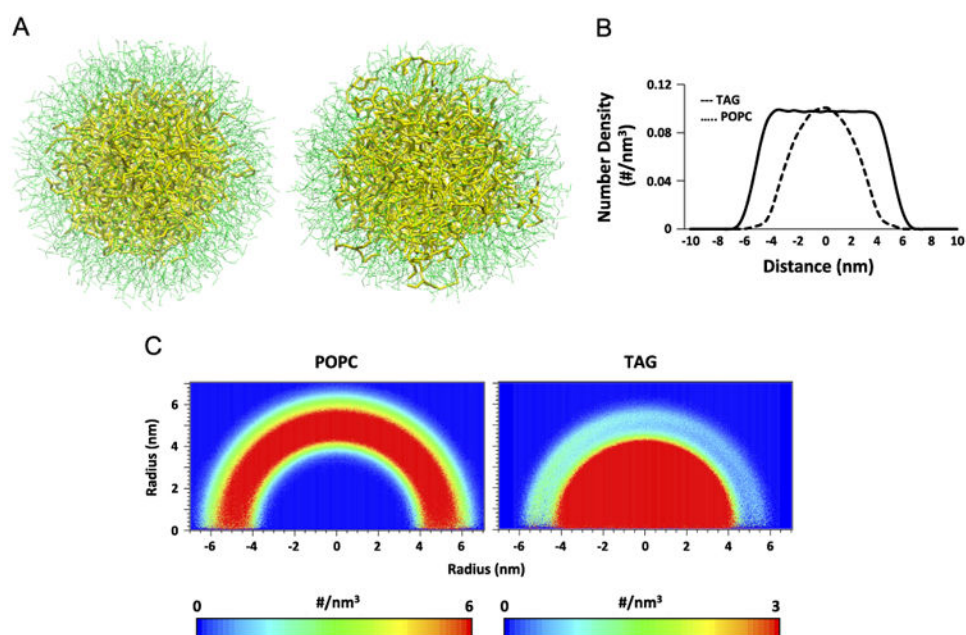
Fig. 4.
CG-MD simulations of lipid droplets with POPC in the surface monolayer and TAGs in the hydrophobic core (in the absence of oxidized lipids–control system). (A) CG-MD snapshot of the control system at t=0 ns (left) and t=2 μs (right). Color guide: thin green line, POPC; thick yellow line, TAG. (B) 1D number density of lipids along the z-axis of the simulation box. (C) 2D number density maps of POPC (left) and TAG (right) molecules along the z direction.
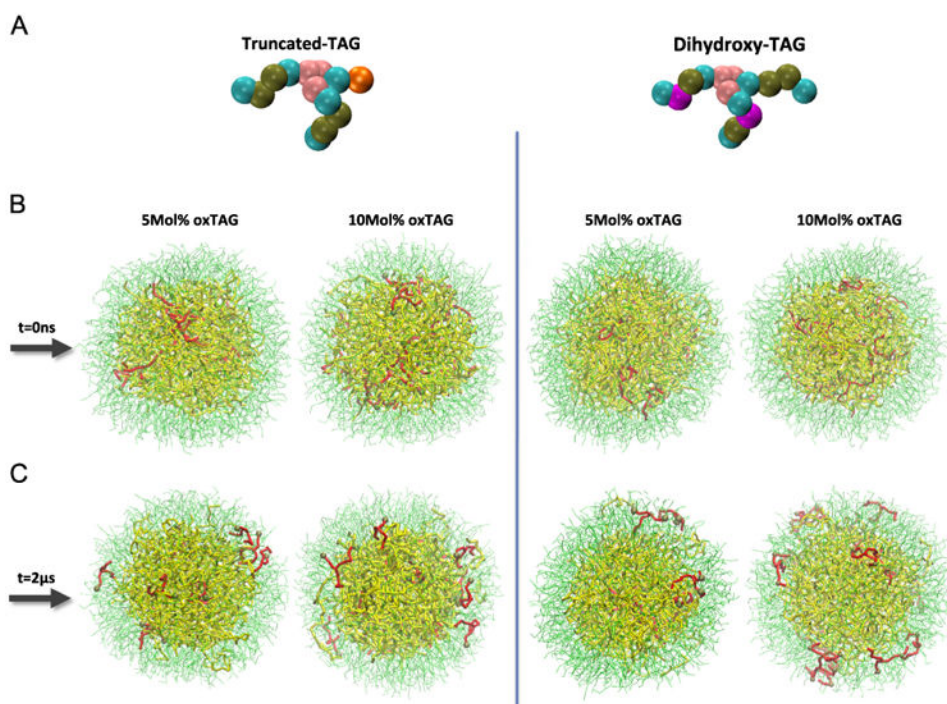
Fig. 5.
Initial and final configurations of LDs demonstrating partitioning of oxTAGs to the phospholipid monolayer. (A) CG models of oxTAG species. Color guide for CG model of oxTAG: cyan, bead containing carbons with sigma bonds (e.g., C-C-C-C); brown, bead containing carbons with sigma and one pi bonds (e.g., C-C-C=C); pink, glycerol group; purple, part of the acyl chain in dihydroxy-TAG containing –OH group; orange, part of acyl chain in oxidatively truncated oxTAG containing =O group. (B and C) Initial and final configurations of LDs structure containing 5 mol% (left) and 10 mol% (right) truncated oxTAGs and dihydroxy oxTAGs. Color guide for LD structure, thin green line, POPC; thick yellow line, TAG; thick red line, oxTAG; brown sphere, oxidized bead.
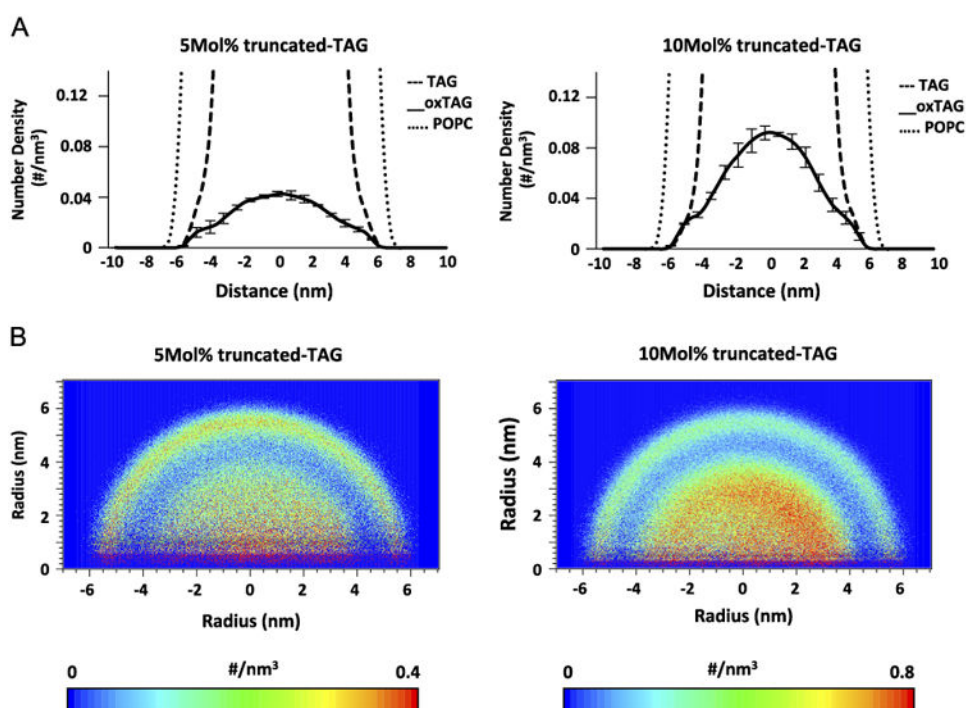
Fig. 6.
Number density of oxTAGs in the systems containing truncated oxTAGs along the *z*-axis of the simulation box. (A) 1D and (B) 2D number density of oxTAGs for systems containing 5 mol% (left) and 10 mol% (right) oxygenated truncated-TAGs.

Table 1

Molecular speciation and fatty acids composition of TAGs in: (i) DCs from tumor-bearing animals, and (ii) hypoxic trophoblasts.

DCs from tumor-bearing animals		Hypoxic trophoblasts	
Molecular species	**Fatty acid composition**	**Molecular species**	**Fatty acid composition**
52:4	C16:0/C18:2/C18:2	52:4	C16:0/C18:2/C18:2
52:3	C16:0/C18:2/C18:1	52:3	C16:0/C18:2/C18:1
52:2	C16:0/C18:1/C18:1	52:2	C16:0/C18:1/C18:1
54:6	C16:0/C18:2/C20:4	54:6	C16:0/C18:2/C20:4
54:5	C18:1/C18:2/C18:2	54:5	C16:0/C18:2/C20:3
54:4	C18:1/C18:2/C18:1	54:4	C16:0/C18:2/C20:2
56:8	C18:1/C18:2/C22:6	56:8	C18:2/C18:2/C20:4
56:7	C16:0/C18:1/C22:6	56:8	C16:0/C18:2/C22:6
56:7	C18:1/C18:2/C20:4	56:7	C18:1/C18:2/C20:4